Nanoscale Horizons

ROYAL SOCIETY OF CHEMISTRY

COMMUNICATION

View Article Online
View Journal

Cite this: DOI: 10.1039/d4nh00174e

Received 23rd April 2024,
Accepted 11th June 2024

DOI: 10.1039/d4nh00174e

rsc.li/nanoscale-horizons

Nanomaterials as a Service (NaaS) concept: on-demand protocols for volume synthesis of nanomaterials†

Stylianos Kioumourtzoglou,*[a] Sebastian Hof,[a] Cécile Kalk,[a] Viktor Toth,[b] Mikaela Görlin,[c] Jaroslava Nováková[d] and Jacinto Sá*[ae]

Establishing scalable nanomaterials synthesis protocols remains a bottleneck towards their commercialisation and, thus, a topic of intense research and development. Herein, we present an automated machine-learning microfluidic platform capable of synthesising optically active nanomaterials from target spectra originating from prior experience, theorised or published. Implementing unsupervised Bayesian optimisation with Gaussian processes reduces the optimisation time and the need for prior knowledge to initiate the process. Using PTFE tubing and connectors enables facile change in reactor design. Ultimately, the platform substitutes the labour-intensive trial-and-error synthesis and provides a pathway to standardisation and volume synthesis, slowing down the translation and commercialisation of high-quality nanomaterials. As a proof-of-concept, Ag nanoplates and Prussian-blue nanoparticle protocols were optimised and validated for volume production.

New concepts

We report a new automated machine-learning microfluidic platform capable of synthesising optically active nanomaterials from target spectra originating from prior experience, theorised or published. The differentiation between the published research is twofold: (i) the use of unsupervised Bayesian optimisation with Gaussian processes to reduce the optimisation time and the need for prior knowledge to initiate the process, and (ii) microfluidic reactors made from PTFE tubing that enables customisation of design at low cost. Eventually, the platform substitutes the labour-intensive trial-and-error synthesis and provides a pathway to standardisation and volume synthesis, slowing down the translation and commercialisation of high-quality nanomaterials. The proposed approach's conceptual advantage is that it enables the production of particles with the same quality and morphology as the optimised protocol in volume and anywhere. Ultimately, the innovation driver is the establishment of the Nanomaterials as a Service (NaaS) concept, where end-users request particles with specific characteristics, and the manufacturer can rapidly optimise a protocol and produce in volume the desired nanomaterial or provide the protocol for production at the end-user site, which is yet to be achieved.

1 Introduction

The discovery and optimisation of nanomaterial synthesis protocols requires a highly skilled and trained labour force. It is, therefore, not surprising that nanomaterial synthesis protocol standardisation and translation to volume production remain significant bottlenecks for nanoparticle commercialisation.[1] Achieving the potential of nanomaterials' application requires developing continuous manufacturing technologies that combine precision, flexibility, and affordability. Innovative manufacturing approaches must ensure morphological control and broad applicability to nanomaterial synthesis to guarantee economic viability.[2] Ultimately, the innovation driver is the establishment of the Nanomaterials as a Service (NaaS) concept, where end-users request particles with specific characteristics, and the manufacturer can rapidly optimise a protocol and produce in volume the desired nanomaterial or provide the protocol for production at the end-user site, which is yet to be achieved.

The exponential growth in nanoscience materials synthesis and theoretical capabilities, allied with open access efforts, reduced the challenge in accessing target data necessary to implement machine-learning approaches to reduce labour-intense synthesis protocol optimisation. However, the development of NaaS concepts remains constrained by two significant challenges: lack of low-cost and flexible reactor design and deficiency in reliable and fast unsupervised optimisation algorithms.

[a] Department of Chemistry-Ångström, Physical-Chemistry Division, Uppsala University, Lägerhyddsvägen 1, Uppsala 751 20, Sweden. E-mail: stylianos.kioumourtzoglou@kemi.uu.se, jacinto.sa@kemi.uu.se
[b] Toptal, LLC, 2810 N. Church St #36879, Wilmington, DE 19802-4447, USA
[c] Department of Chemistry-Ångström, Structural Chemistry Division, Uppsala University, Lägerhyddsvägen 1, Uppsala 751 20, Sweden
[d] Department of Surface and Plasma Science, Charles University, V holesovickach 2, Prague 8, 18000, Czech Republic
[e] Institute of Physical Chemistry, Polish Academy of Sciences, Marcina Kasprzaka 44/52, Warsaw 01-224, Poland

† Electronic supplementary information (ESI) available. See DOI: https://doi.org/10.1039/d4nh00174e

Regarding reactor design, microfluidics have emerged as a powerful tool for producing high-quality nanoparticles.[3–6] However, microfluidic systems often use pre-established reactor geometries called reactor chips. Their design geometry rigidity demands significant prior knowledge from the user when selecting them or extensive trial-and-error attempts that are unsustainable and expensive. Furthermore, chip integrity, resistance to fouling and ageing are also things to be considered, especially when running unsupervised optimisations. These issues can be mitigated with routine cleaning processes (increasing the optimisation time)[7] and multi-point analysis of the reactor's health (increasing cost and complexity).[8] Additionally, to be effective, the multi-point analysis must be fast and non-invasive, reducing the range of analytics to in-line optical methods that might not be sensitive to the species, causing reactor fouling or ageing. Therefore, when it comes to reactors, their geometry should be changeable and adaptable, made of durable fouling-resistant materials, easy to integrate with pumping and analytical systems, and cost-effective.

The growing interest in machine learning as a problem-solving tool led to the rapid proliferation and development of optimisation algorithms to a level that has become a deterrent to nano-innovators' use due to the overwhelming amount of choice. The decision of which method to use often comes from weighing the following parameters: how big is the parameter space, how continuous the process is, how much prior knowledge the user has, and how fast it converges. The latter does not relate to the time it takes to optimise, but the number of data points one must acquire to get the desired result.

A large class of nanomaterials manufacturing uses kinetically controlled synthesis methods, where particles are made from precursor salts, reducing or oxidising chemicals and growth-directing agents. Examples of nanomaterials produced *via* this approach include plasmonic nanoparticles, semiconductors, quantum dots, *etc.*[9] Their synthesis has a characteristically low number of continuous control parameters (less than ten) that are easy to generate data points, making them particularly suitable for Bayesian optimisation with Gaussian processes. Bayesian optimisation with Gaussian processes is an unsupervised algorithm that converges fast and requires relatively low computational power.

This communication reports a development that quells bottlenecks surrounding the discovery, optimisation, standardisation and development of the NaaS concept to fabricate high-quality nanomaterials. The workflow is schematically representation in Fig. 1. The optimised protocols consist of the exact pump flows with specific substrate concentrations and the reactor configuration, which should be transferable to any production facility.

As a proof-of-concept, we optimised and standardised protocol for synthesising plasmonic silver nanoplates and Prussian blue nanoparticles, demonstrating the breadth of materials that can be produced with the presented approach. Plasmonic nanoparticles can capture and concentrate distant radiation within subwavelength regions defies diffraction limits,[10,11] resulting in powerful near-fields, hot carriers and localised heat,[12,13] which spurred the development applications in biosensing,[14] cancer therapy,[15] photovoltaic,[16,17] photodetectors,[18] catalysis,[19,20] emitting devices,[21,22] solar energy converters,[23] among others. Prussian blue, which people also call ferric ferrocyanide, is used in catalysis,[24] hydrogen storage,[25] photochemistry,[26] chemical and bio-sensors,[27] clinical medicine,[28] and most promisingly, high crystalline Prussian blue analogues are used as a cathode on sodium-ion batteries.[29,30]

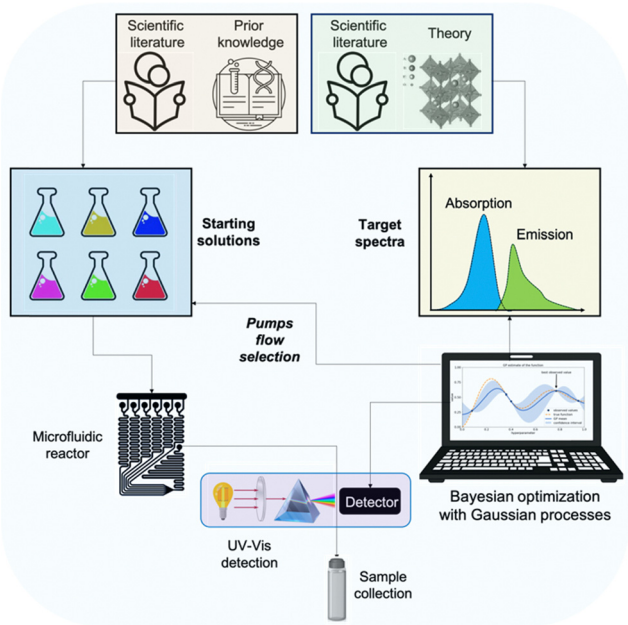

Fig. 1 Schematic workflow representation for optimising a synthesis protocol with the proposed approach.

2 Results and discussion

2.1 Reactor design

The main components of the hardware were reported elsewhere.[7] Briefly, four continuous syringe pumps draw liquid with specific chemicals necessary for the synthesis and an in-flow UV-Vis absorbance detection (Ocean Insight).

Polytetrafluoroethylene (PTFE) is a hydrophobic, non-wetting, high-density, resistant to high temperatures (m.p. 327 °C), versatile and best known for its non-stick properties material. These properties make PTFE an ideal reactor material. Additionally, PTFE tubes with 1/16″ outer diameter (OD) can be bought with a variable inner diameter (ID) ranging from 0.2–1 mm, ideally suited for microfluidics. The fix OD enables easy connectivity through T and cross-tube fitting connections and offers constant connector dimensions to pumps, the detection system and the reactor. Maintenance costs are dramatically reduced for new tubing and connectors. This versatility and variety permit the creation of tailor-made reactor geometries and continuous experimentation and optimisation of the geometry, as demonstrated by the proof-of-concept examples herein. The precise description of the reactor used

for each proof-of-concept synthesis is shown in the Sections 2.3 and 2.4.

2.2 Optimization algorithm

The method of Bayesian optimization with Gaussian processes was applied to determine the optimal pump settings necessary to achieve the target optical spectrum of nanoparticles. This technique is advantageous for quickly approaching an optimal solution with minimal sampling, hence its use in this context. The general settings of Bayesian optimisation can be found in Maggi tutorial.[31]

Our goal in employing Bayesian optimization is to understand and optimize an unknown function $f(x)$ based on sampled data. We postulate that observations might be noisy, such that an observed value $f(x)$ equals the true function value plus an error term ε, where the expected value of ε is zero and independent across samples, *i.e.*,

$$\text{Goal: } \max_{x\in\chi} f(x), \quad \chi \subset \mathbb{R}^k$$

$f(x)$ is unknown; f is learnt *via* sampling (deploy $x \rightarrow$ observe $f(x)$); optional: observations are noisy (deploy $x \rightarrow$ observe, $\tilde{f}(x) = f(x) + \varepsilon$ where $\mathbb{E}[\varepsilon] = 0$ and must be independent across different samples.

The process involves the following steps: at any given step n, after observing the pairs $(x_1, f(x_1)),\ldots,(x_n,f(x_n))$, we infer the function f at new points not in the existing observations using a Gaussian process. This yields a normal distribution for each untested point, characterized by a calculated mean and variance. We then select the next point $x_n + 1$ to sample by maximizing an acquisition function $g(x)$ which considers both the mean and variance, effectively balancing between exploring new areas and exploiting known ones. An example of such an acquisition function is the upper confidence bound (UCB). After selecting $x_n + 1$, we observe and record the new noisy sample $f(x_n + 1))$.

The choice of Bayesian optimization is justified for nanoparticle synthesis due to the typically small number of controllable parameters, usually less than 10, such as chemical concentrations and temperatures. The continuous nature of $f(x)$, reflecting changes in spectral outputs with variations in synthesis conditions, supports the use of this method. Additionally, the frequency of updating x is deliberately low to manage computational load, though this can be adjusted for faster synthesis methods like hot injections.

In summary to use Baysien optimization for nanomaterials synthesis it must keep on the following aspects:

- Small number k of control parameters, as a rule of thumb $k < 20$ because a nonconvex problem in $\mathbb{R}^k$ is solved to choose the next point x_n. This condition is easily fulfilled in nanoparticle synthesis since the variables are chemicals and temperature used, which rarely exceeds 10 controllable parameters.
- f is continuous for the Bayesian optimization to leverage the fact that for $x \approx x' \rightarrow f(x) \approx f(x')$. This is also valid in most syntheses since small changes in reactant concentrations rarely produce completely different nanoparticle outputs.
- $\tilde{f}(x)$ is defined as the measured spectral fit at control parameters x to the target spectrum. The fit of two spectra may be defined in various ways to establish a continuous function f.
- x is updated at a low frequency because deciding the next point x_n is a computationally intensive task. This is once more easily achievable in kinetically controlled synthesis processes but might require the introduction of time stamps for faster synthesis procedures, such as hot injections commonly used in quantum dot synthesis.
- Bayesian optimisation can use prior knowledge, such as historical data and/or knowledge, to speed up the process.

In this context, a Gaussian process helps model the uncertainty about $f(x)$, considering all previous samples to predict the function's behavior at unsampled points. The computation of the mean and variance for each point is automated, using the prior mean mx and the kernel function $K(x,x')$ which ideally represents the covariance between sampled points.

In the present case, the unknown $f(x)$ is modelled as a Gaussian process. Given previous samples $\tilde{f}(x_1),\ldots,\tilde{f}(x_n)$, one can infer $f(x)$ for any $x \in \mathcal{X}$ *via* the Gaussian process posterior. As such, at every point $f(x)$ a normal distribution is obtained with a mean and variance predicted. Briefly, given a collection of jointly Gaussian random variables, there is an elegant way to compute the probability of an unknown variables subset from an observable subset through a Gaussian posterior expressed as:

$$p\left(y_A \vdots y_B\right) = \mathcal{N}\left(\mu_A + \Sigma_{AB}\Sigma_B^{-1}(y_A - \mu_B), \quad \Sigma_A - \Sigma_{AB}\Sigma_B^{-1}\Sigma_{AB}^T\right)$$

$$y_A = f(x)$$

$$y_B = [\tilde{f}(x_1),\ldots,\tilde{f}(x_n)]$$

where, μ and Σ are the averages and covariance matrixes, respectively. The compute of μ and Σ are done in an automated way using the following expressions:

Prior mean

$$m(x),\ \forall x \in \mathcal{X}.\ \text{Ideally},\ m(x) = \mathbb{E}\left[\tilde{f}(x_n)\right] = f(x)$$

Kernel function

$$K(x,x').\ \text{Ideally},\ K(x,x') = \text{Cov}(f(x),f(x'))$$

Lastly, the integration of Bayesian optimization allows for the inclusion of diverse data sources including historical, published, and theoretical data, enabling robust exploration of the parameter space to quickly assess the proximity of the optimum to the available chemical and temperature conditions. This process is facilitated by the parallel execution of deployment and function inference steps, enhancing the efficiency of the optimization process.

Maggi's tutorial provides a detailed explanation of how this is computed.[31] The code was written in Python, which is also used to integrate the hardware and analytics.

2.3 Synthesis of Ag nanoplates

This study reports the synthesis of two kinds of particles (Ag nanoplates and nano-Prussian blue) that require different reactor designs and configurations to confirm the proposed approach's potential breath. Starting with Ag nanoplates, the batch protocol developed by Aherne *et al.*[32] was used as inspiration. This seed-mediated Ag nanoparticle synthesis utilises pre-made seeds mixed with ascorbic acid (reducing agent) and $AgNO_3$ (Ag salt). An additional pump was used to supply the capping agent after the synthesised particles, in this case, citrate.

The seeds were prepared manually because the process is relatively simple and rapid. Moreover, using $NaBH_4$ (unstable reactant) and the light colour of the seed solution make optimisation using the approach described herein challenging. The protocol for Ag seed production is described in the Methods section. The quality of the seeds was evaluted by dynamic light scattering (DLS) prior to use to confrim they have the correct size.

The reactor layout used for synthesising the Ag nanoplates is shown in Fig. 2a. Pump channel 3 contains the seeds solution diluted 1 : 10, mixed with the 1 mM ascorbic acid (pump channel 4) *via* a T-junction connector. The chemicals are combined on a 30 cm 1/16″ PTFE tube with an ID of 500 μm. After the mixing part, 0.5 mM of $AgNO_3$ is added through pump channel 2. The components are reacted on a 200 cm 1/16″ PTFE tube with an ID of 500 μm. The formed particles are capped with citrate, added after the reaction *via* pump channel 1 (trisodium citrate 25 mM). The nanoparticle capping occurs in a 40 cm 1/16″ PTFE tube with an ID of 500 μm.

The quality of the particles is analysed *via* online UV-Vis spectrometry through a Z-cell unit and compared to a pre-loaded spectrum of the desired target particles. Several protocols were established and scored using Bayesian optimisation with Gaussian processes. Each protocol has a unique set of pump flows. The highest-scoring protocol (*i.e.* the best fit) is summarised in Table 1.

Fig. 2b shows the optical image of the particle prepared with the optimised protocol, consistent with a UV-Vis spectrum with an absorption maximum centred at 645 nm (ESI,† Fig. S1). The DLS measurement revealed two peaks (Fig. 2c), one corresponding to 2.0 nm and another to 43.8 nm. Transmission

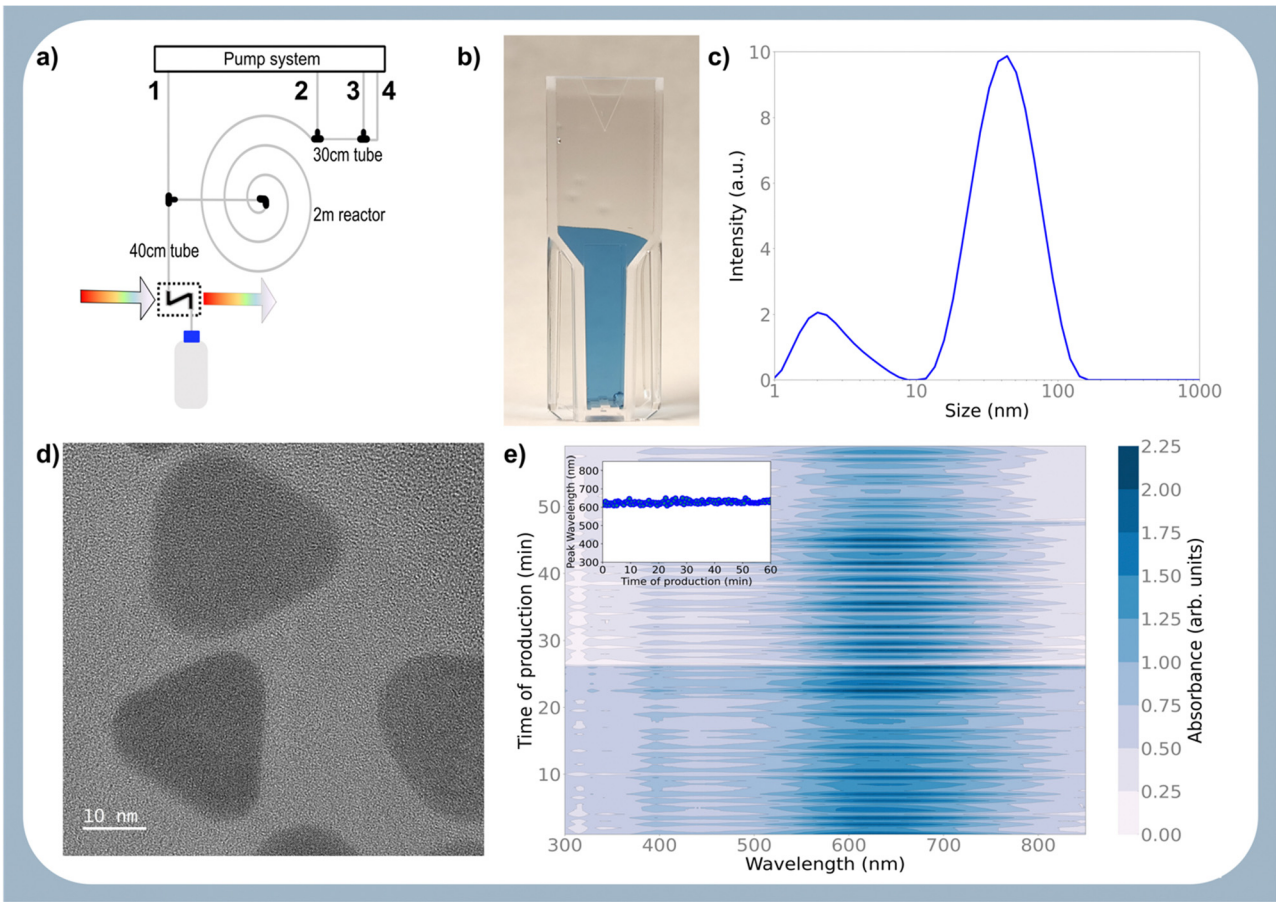

Fig. 2 Summary of the reactor design and characterisation of Ag nanoplates produced. (a) Schematic of the reactor design used for the synthesis of Ag nanoplates [Pump channels chemicals → 1 = trisodium citrate [25 mM]; 2 = $AgNO_3$ [0.5 mM]; 3 = seeds [1 : 10]; 4 = ascorbic acid [1 mM]]; (b) optical photograph of the optimized Ag nanoplates; (c) DLS of the optimised Ag nanoplates; (d) TEM of the Ag nanoplates, and (e) UV-Vis spectra of the Ag nanoplates during 1 h production using the optimised protocol. The inset shows the position of the absorption maximum over time.

Table 1 Summary of the optimised pump flows for synthesising Ag nanoplates

Pump channel	Chemicals [concentration]	Flow rate (μL min^{-1})
1	Trisodium citrate [25 mM]	49.0
2	$AgNO_3$ [0.5 mM]	132.0
3	Seeds [1 : 10]	101.0
4	Ascorbic acid [1 mM]	237.0

electron microscopy (TEM) shown in Fig. 2d reveals that the particles are Ag nanoplates with triangular shapes, as expected from Aherne *et al.*[32] studies. The triangle side lengths are between 30–40 nm. The discrepancy with the size estimated from DLS is that DLS only measures the hydrodynamic radius and TEM for the metallic core. The second peak in the DLS is related to the nanoplate thickness, responsible for the UV-Vis absorption peak at around 401 nm (see Fig. S1, ESI†).

The absorption spectrum of the optimized Ag nanoplates protocol is consistent with the spectrum of the nanoparticles produced using the Aherne *et al.*[32] batch protocol (see Fig. S1, ESI†). In both cases, the Ag^+ ions are fully consumed based on X-ray fluorescence (XRF) analysis of the supernatant and the observation that unreacted Ag^+ ions left in a synthesizing solution will be slowly added to the nanoplates increasing the particle size. However, UV-Vis absorption and DLS analysis after 15 days showed no change in optical absorption and size.

Having established that all the silver ions are completely consumed in both syntheses, the process's yield for metal consumption is 100%. However, as is noticeable in Fig. S1 (ESI†), the optical absorption intensity is different for both methods. The absorption intensity at the maximum in solutions after synthesis reflects the nanoparticle concentration in the solution. In the case of the batch, the peak has a net intensity of 0.74 *versus* 0.36 for the ones produced in the microfluidic reactor. The batch process generates about 1 mL min^{-1} of Ag NPs, but it is challenging to scale up production because insufficient stirring creates inhomogeneity in the solution, increasing particle polydispersity. The microfluidic reactor generates nanoparticles at a rate of *ca.* 0.5 mL min^{-1} but continuously and reproducibly. This is the proposed approach's conceptual advantage; it enables the production of nanomaterials with the same quality and morphology as the optimised protocol in volume and anywhere.

To demonstrate this, the reactor was configured with the same geometry, and the pump flows were set to the optimised values. The system was allowed to produce particles with these settings for 1 h, and the output was monitored *via* online UV-Vis. As shown in Fig. 2e, the reactor produced particles with the same optical absorption without noticeable reactor degradation due to fouling or blockage. This is even more evident from the Fig. 2e inset showing the position of the absorption maximum over time, which is very sensitive to changes in particle morphology. The quality of the particles is similar to the ones offered by commercial vendors,[33] with the added benefit that the settings can be used in any lab or industrial plant to synthesise this optimised protocol. This is the competitive edge of the proposed approach.

2.4 Synthesis of Prussian blue nanoparticles

The system produced Prussian blue nanoparticles to demonstrate the approach's applicability to other materials. In this case, a batch protocol proposed by Shokouhimehr *et al.*[34] inspired the optimisation. The reactor layout used for synthesising the Prussian blue nanoparticles is shown in Fig. 3. In this situation, a three-channel system was used. Pump channel 1 contains a 25.5 mM citric acid solution mixed with 1.0 mM of $FeCl_3$ (pump channel 2) *via* a T-junction connector. The chemicals are homogenised on a 40 cm 1/16″ PTFE tube with an ID of 500 μm that is heated to 60 °C. After the mixing part, a 1 mM $K_4[Fe(CN)_6]x\ 3H_2O$ + 25.5 mM citric acid mixture is added *via* pump channel 3, and the reaction mixture reacts on a 40 cm 1/16″ PTFE tube with an ID of 500 μm that is heated to 60 °C. The reaction is further aged on a 200 cm 1/16″ PTFE tube with an ID of 500 μm at room temperature before the reaction of the analytics. Any potential HCN gas formed during the synthesis is hydrolysed with a concentrated solution of KOH. The formation of HCN is possible since the average reaction pH is around 2.8.

The quality of the particles is analysed *via* online UV-Vis spectrometry through a Z-cell unit and compared to a preloaded spectrum of the desired target particles. Several protocols were established and scored using Bayesian optimisation with Gaussian processes. Each protocol has a unique set of pump flows. The best-fit protocol is summarised in Table 2.

Fig. S2 (ESI†) shows the UV-Vis spectrum of the optimised nanoparticles with an absorption maximum centred at 697 nm, consistent with the formation of Prussian blue nanomaterial.[35] The TEM of the prepared particles is shown in Fig. 4a, revealing small particles that are relatively uniform in size and shape. The histogram in Fig. 4b shows that particles are about 7.2 ± 1.3 nm, a uniformity in size confirmed by DLS analysis (Fig. S3, ESI†). The

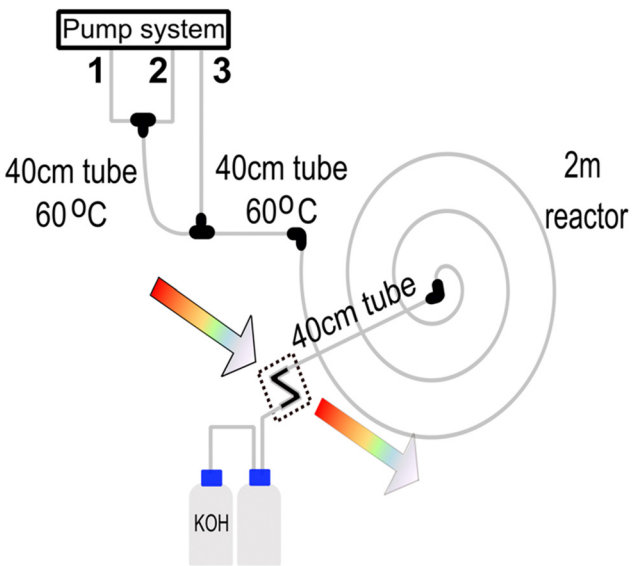

Fig. 3 Schematic representation of the microfluidic reactor designed to produce Prussian blue nanoparticles. Pump channels chemicals → 1 = citric acid [25.5 mM]; 2 = $FeCl_3$ [1 mM]; 3 = $K_4[Fe(CN)_6]x\ 3H_2O$ [1 mM] + citric acid [25.5 mM].

Table 2 Summary of the optimized pump flows for synthesizing Prussian blue nanoparticles

Pump channel	Chemicals [concentration]	Flow rate ($\mu L\ min^{-1}$)
1	Citric acid [25.5 mM]	220.0
2	$FeCl_3$ [1 mM]	134.0
3	$K_4[Fe(CN)_6]x\ 3H_2O$ [1 mM] + citric acid [25.5 mM]	137.0

discrepancy between the average size estimated from DLS and TEM data is related to what is measured with each technique, as highlighted when presenting the Ag nanoplates data. The Prussian blue nanoparticle structure was determined by powder X-ray diffraction (XRD) shown in Fig. S4 (ESI†), which revealed the characteristic cubic framework built from Fe(II)–C–N–Fe(III) sequences, consistent with what has been published.[36] As with the Ag nanoplates protocol, once optimized, the protocol was used to synthesize large batches of samples to be tested in applications like batteries and oxygen evolution reactions.

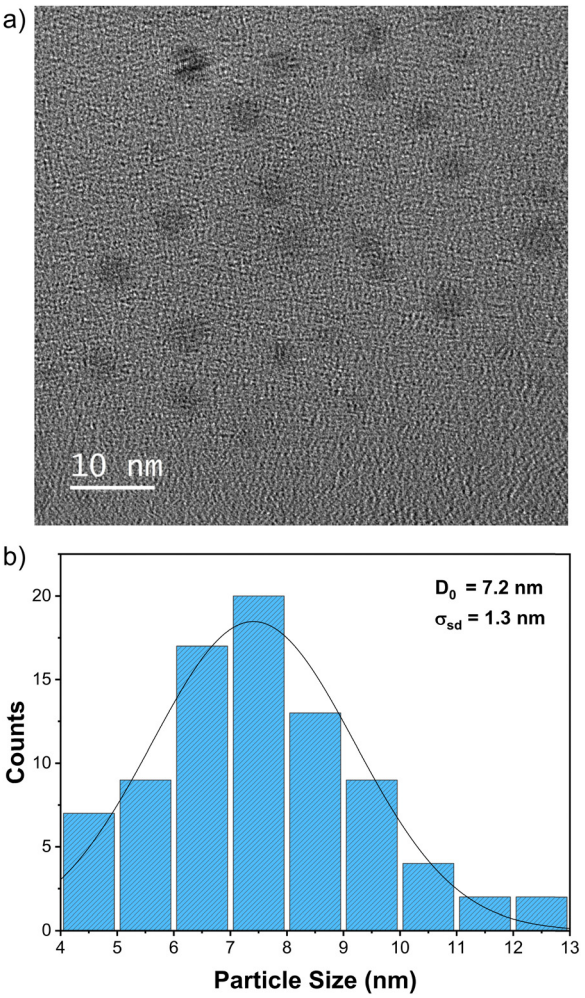

Fig. 4 TEM of the Prussian blue nanoparticles produced with the optimised synthesis protocol. (a) Representative TEM image; (b) histogram showing the distribution of particle sizes.

The concentration of Prussian blue synthesized can be estimated from the optical absorption. Considering that the produced Prussian blue solution had an optical absorption at 700 nm of *ca.* 0.7 and the molar absorption coefficient at this wavelength is $3.0 \times 10^4\ M^{-1}\ cm^{-1}$,[37] this equates to a concentration of 0.023 mM of Prussian blue. The reactor produces particles at a rate of about 0.5 mL min^{-1}, equating to 8.4×10^{-8} mol of Fe per min in the product considering the formula $C_{18}Fe_7N_{18}$. Considering the amount of iron used per minute, one estimates a yield concerning the metal of about 30%.

2.5 Final considerations

Having demonstrated the system's applicability, it is relevant to provide some consideration with respect to system limitations and how one could establish a commercial NaaS concept.

The current iteration of the proposed reactor permits reactions up to 3 bar pressure and 150 °C (limited by the heating system). For example, Au nanospheres with a diameter of *ca.* 8 nm at 85 °C (see ESI,† for reactor scheme Fig. S5 and the characteristic UV-Vis (Fig. S6) and DLS (Fig. S6) data). However, the approach can be adapted to high-pressure and high-temperature synthesis by replacing the tubing material with stainless steel and implementing more advanced heating and pressure regulator systems, which are commercially available.[38] In this respect, the limitations are primarily related to available budgets and user willingness to handle more complex and sophisticated hardware. During the discovery and optimization stage, materials with the wrong properties are generated, which can induce reactor fouling and clogging. Thus, when possible, it is advisable to use cheaper and less prone to-fouling reactor tubing materials, like PTFE and PFA.

The unsupervised Bayesian optimization with Gaussian processes reduces the optimization time and the need for prior knowledge to initiate the process. However, the optimization algorithm is limited to twenty optimization parameters, and the math becomes computationally expensive once we go over ten parameters. However, considering the published wet chemical synthesis protocols, this is not a significant impediment because the protocols often use less than ten parameters.

A commercial NaaS concept can take several dimensions, which are difficult to cover in their entirety. However, we would like to mention three examples of how this could be beneficial.

Bulk synthesis of specialized nanoparticles. as aforementioned, one of the current bottlenecks is the commercialization of specialized nanoparticles, which were discovered using small-scale wet batch processes. If the process can be adapted to flow, then the proposed approach could be implemented to find and optimize a protocol for the synthesis of such particles. Once this step is accomplished, a standard procedure is established for the nanoparticle production and, consequently, used to manufacture bulk amounts, as shown we have shown herein for the Ag nanoplates and Prussian blue nanoparticles.

Synthesis of unstable nanoparticles on demand. There are many examples of unstable nanoparticles, such as transport. A possible solution is to manufacture them close to their

application site. In such a case, the proposed approach herein could be used in the first instance to discover, optimise, and standardise protocols for producing high-quality nanomaterials. The protocol, including reactor design and components, would be subsequently replicated at the customer site, enabling on-demand *in situ* manufacturing and suppressing issues related to the translation to industrial settings.

Discovery of translational protocols for new materials. the first two examples relate to solving problems surrounding the translation of known nanomaterials. However, the proposed approach can also be used to discover new materials that fulfill the end customer's requirements. For example, caesium lead halide perovskite nanomaterials have been developed for a plethora of applications due to their exciting optical properties.[39,40] However, one can imagine applications in which the use of lead would not be tolerated due to its known toxicity. Therefore, the end-user could request a NaaS company to find an alternative to the lead-based material that does not contain lead but preserves the specific properties of interest. Once more, if the protocol is established, not only would we have new lead-free material but also a translational and scalable way to manufacture this new material.

Using the proposed approach to changing the current industrial manufacturing nanomaterials landscape is challenging, even when presented with cheaper, more adaptable, and more sustainable methods. This is because existing producers have established production lines, often involving significant capex expenditure and hired staff with specialization in such methods. Therefore, the use of a new approach will find more substantial penetration in unscaled, underdeveloped, and to-be-discovered processes. However, if one can identify a material producer willing to disrupt, the proposed approach could circumvent potential limitations with already commercialized nanoparticles. For example, establishing alternative flow protocols to batch process enables modularization. Modular concepts that can be produced in series allow for cost-efficient production through economies of scale. As their systems and components can be factory-assembled, they can be transported as modules or whole units to a location, reducing installation costs. However, one needs to examine processes individually and account for the end-user cost limitations and the pain associated with modifying the current production method, which is out of this work scope.

3 Conclusions

This contribution provides a solution for discovering, developing, optimising, and standardising nanoparticle synthesis protocols. The hardware is based on microfluidic reactors, which can be customised and tailored to specific nanomaterials synthesis. This approach's versatility and low cost make the reactor design one of the possible optimisation parameters accessible to most users. The protocols are optimised using Bayesian optimisation with Gaussian processes, ideally suited for nanomaterials synthesis because it ensures rapid and reliable convergence. The standardised protocols could be used for large-scale production, which can be achieved for parallel reactor assemblies using prior optimised protocols, circumventing the existing bottleneck of nanomaterials translation to commercial applications. Notably, the concept paves the way for the creation of Nanomaterials as a Service (NaaS) business models, a future application where nanomaterials customers can request specific materials that are optimised and standardised by specialised NaaS companies, effectively decoupling discovery and standardisation from large-scale production.

4 Methods

4.1 Protocol for Ag seeds production

We adopted the protocol reported by Aherne *et al.*[32] Briefly, the protocol for seed production is as follows: silver seeds are produced by combining aqueous trisodium citrate (5 mL, 2.5 mM), aqueous poly(sodium styrene sulphonate) (0.25 mL, 500 mg L^{-1}; 1000 kDa) and aqueous $NaBH_4$ (0.3 mL, 10 mM, freshly prepared) followed by addition of aqueous $AgNO_3$ (5 mL, 0.5 mM) at a rate of 2 mL min^{-1} under vigorous stirring.

4.2 Nanomaterials characterisation

The quality of the particles produced with optimised protocols was assessed with UV-Vis spectrometry, dynamic light scattering (DLS) and transmission electron microscopy (TEM). The DLS measurements were performed with a Zetasizer Nano ZS from Malvern Ltd. The UV-Vis absorbances were determined on a Cary 5000 UV-Vis. The morphology and structure of the nanoparticles were characterised by employing transmission electron microscopy (TEM) in high-resolution mode (HRTEM), using a JEOL JEM-2200FS microscope operating at an accelerated voltage of 200 kV. The point resolution in HRTEM mode is down to 0.19 nm (lattice resolution of 0.10 nm). Specimens were prepared by placing a drop of the dispersion of the particles in distilled water on a 300-mesh copper grid covered by a lacey carbon film (Agar Scientific). The post-processing of the acquired images was done using Digital Micrograph software.

Data availability

The data related to the figures in the paper available from the corresponding author upon request.

Conflicts of interest

The authors declare that there are no conflicts to declare.

Acknowledgements

The authors would like to acknowledge the ÅForsk foundation (grant no. 23-268), ReMade-at-ARI (grant no. PID27203), and the Physical Chemistry division of the Department of Chemistry-Angstrom, Uppsala University, for their financial support.

Notes and references

1 Global Nanoparticles Market in Biotechnology and Pharmaceutical Sectors, 2017–2021, 2017, **https://news.marketersmedia.com/nanoparticles-market-in-biotechnology-and-pharmaceutical-sectors-2017-global-market-expected-to-grow-at-cagr-21-72-and-forecast-to-2021/270564**. Accessed on April the 17th, 2024.
2 H. Zhao, W. Chen, H. Huang, Z. Sun, Z. Chen, L. Wu, B. Zhang, F. Lai, Z. Wang, M. L. Adam, C. H. Pang, P. K. Chu, Y. Lu, T. Wu, J. Jiang, Z. Yin and X.-F. Yu, *Nat. Synth.*, 2023, **2**, 505.
3 S. Marre and K. F. Jensen, *Chem. Soc. Rev.*, 2010, **39**, 1183.
4 J. Nette, P. D. Howes and A. J. deMello, *Adv. Mater. Technol.*, 2020, **5**, 2000060.
5 S. Krishnadasan, R. J. C. Brown, A. J. deMello and J. C. deMello, *Lab Chip*, 2007, **7**, 1434.
6 X. Xie, Y. Wang, S.-Y. Siu, C.-W. Chan, Y. Zhu, X. Zhang, J. Ge and K. Ren, *Biomicrofluidics*, 2022, **16**, 041301.
7 D. L. A. Fernandes, C. Paun, M. V. Pavliuk, A. B. Fernandes, E. L. Bastos and J. Sa, *RSC Adv.*, 2016, **6**, 95693.
8 B. Pinho and L. Torrente-Murciano, *Adv. Energy Mater.*, 2021, **11**, 2100918.
9 Y. Wang, J. he, C. Liu, W. H. Chong and H. Chen, *Angew. Chem., Int. Ed.*, 2015, **54**, 2022.
10 L. Novotny and B. Hecht, *Principles of Nano-Optics*, Cambridge University Press, New York, 2006.
11 S. A. Maier, *Plasmonics: Fundamentals and Applications*, Springer, New York, 2007.
12 N. J. Halas, S. Lal, W. Chang, S. Link and P. Nordlander, *Chem. Rev.*, 2011, **111**, 3913.
13 C. Clavero, *Nat. Photonics*, 2014, **8**, 95.
14 H. Xu, E. J. Bjerneld, M. Käll and L. Börjesson, *Phys. Rev. Lett.*, 1999, **83**, 4357.
15 D. P. O'Neal, L. R. Hirsch, N. J. Halas, J. D. Payne and J. L. West, *Cancer Lett.*, 2004, **209**, 171.
16 H. A. Atwater and A. Polman, *Nat. Mater.*, 2010, **9**, 205.
17 F. P. García de Arquer, A. Mihi, D. Kufer and G. Konstantatos, *ACS Nano*, 2013, **7**, 3581.
18 M. W. Knight, H. Sobhani, P. Nordlander and N. J. Halas, *Science*, 2011, **332**, 702.
19 S. Mubeen, L. Lee, N. Singh, S. Krämer, G. D. Stucky and M. Moskovits, *Nat. Nanotechnol.*, 2013, **8**, 247.
20 X. Shi, K. Ueno, T. Oshikiri, Q. Sun, K. Sasaki and H. Misawa, *Nat. Nanotechnol.*, 2018, **13**, 953.
21 A. G. Curto, G. Volpe, T. H. Taminiau, M. P. Kreuzer, R. Quidant and N. F. van Hulst, *Science*, 2010, **329**, 930.
22 L. Novotny and N. van Hulst, *Nat. Photonics*, 2011, **5**, 83.
23 J. W. Schwede, I. Bargatin, D. C. Riley, B. E. Hardin, S. J. Rosenthanl, Y. Sun, F. Schmitt, P. Pianetta, R. T. Howe, Z.-X. Shen and N. A. Melosh, *Nat. Mater.*, 2010, **9**, 762.
24 N. A. Sitnikova, M. A. Komkova, I. V. Khomyakova, E. E. Karyakina and A. A. Karyakin, *Anal. Chem.*, 2014, **86**, 4131.
25 J. Jiménez-Gallegos, J. Rodriguez-Hernandez, H. Yee-Madeira and E. Reguera, *J. Phys. Chem. C*, 2010, **114**, 5043.
26 D. M. Pajerowski, J. E. Gardner, F. A. Frye, M. J. Andrus, M. F. Dumont, E. S. Knowles, M. W. Meisel and D. R. Talham, *Chem. Mater.*, 2011, **23**, 3045.
27 A. A. Karyakin, O. V. Gitelmacher and E. E. Karyakina, *Anal. Chem.*, 1995, **67**, 2419.
28 G. Fu, W. Liu, Y. Li, Y. Jin, L. Jiang, X. Liang, S. Feng and Z. Dai, *Bioconjugate Chem.*, 2014, **25**, 1655.
29 W. J. Li, C. Han, G. Cheng, S.-L. Chou, H.-K. Liu and S.-X. Dou, *Small*, 2019, **15**, 1900470.
30 S. Qui, Y. Xu, X. Wu and X. Ji, *Electrochem. Energy Rev*, 2022, **5**, 242.
31 L. Maggi, 'A tutorial on Bayesian optimization with Gaussian processes', **https://www.lincs.fr/events/a-tutorial-on-bayesian-optimization-with-gaussian-processes/**. Accessed on April the 17th, 2024.
32 D. Aherne, D. M. Ledwith, M. Gara and J. M. Kelly, *Adv. Funct. Mater.*, 2008, **18**, 2005.
33 **https://nanocomposix.com/collections/shape-plates/material-silver**. Accessed on April the 17th, 2024.
34 M. Shokouhimehr, E. S. Soehnlen, J. hao, M. Griswold, C. Flask, X. Fan, J. P. Basilion, S. Basu and S. D. Huang, *J. Mater. Chem.*, 2010, **20**, 5251.
35 R. J. Mortimer and J. R. Reynolds, *J. Mater. Chem.*, 2005, **15**, 2226.
36 F. Shiba, U. Mameuda, S. Tatejima and Y. Okawa, *RSC Adv.*, 2019, **9**, 34589.
37 J. A. Nóbrega and G. S. Lopes, *Talanta*, 1996, **43**, 971.
38 For example: **https://www.vapourtec.com/products/r-series-flow-chemistry-system-overview/**. Accessed on 31/05/2024.
39 L. Protesescu, S. Yakunin, M. I. Bodnarchuk, F. Krieg, R. Caputo, C. H. Hendon, R. X. yang, A. Walsh and M. V. Kovalenko, *Nano Lett.*, 2015, **15**, 3692.
40 R. Begum, X. Y. Chin, B. Damodaram, T. J. N. Hooper, S. Mhaisalkar and N. Mathews, *ACS Appl. Nano Matter.*, 2020, **3**, 1766.

